Theoret. Comput. Fluid Dynamics (2004)
Digital Object Identifier (DOI) 10.1007/s00162-004-0129-1

Theoretical and Computational Fluid Dynamics

Original article

Complex dynamics in double-diffusive convection

Esteban Meca[1], Isabel Mercader[2], Oriol Batiste[2], Laureano Ramírez-Piscina[1]

[1] Departament de Física Aplicada, Universitat Politècnica de Catalunya, Doctor Marañón 44, 08028 Barcelona, Spain
[2] Departament de Física Aplicada, Universitat Politècnica de Catalunya, Jordi Girona 1–3, 08034 Barcelona, Spain

Received October 15, 2003 / Accepted May 25, 2004
Published online September 17, 2004
Communicated by H.J.S. Fernando

Abstract. The dynamics of a small Prandtl number binary mixture in a laterally heated cavity is studied numerically. By combining temporal integration, steady state solving and linear stability analysis of the full PDE equations, we have been able to locate and characterize a codimension-three degenerate Takens–Bogdanov point whose unfolding describes the dynamics of the system for a certain range of Rayleigh numbers and separation ratios near $S = -1$.

Key words: natural convection, binary mixture, nonlinear dynamics, Takens–Bogdanov bifurcation
PACS: 44.25.+f, 47.20.Bp, 05.45.-a

1 Introduction

Double-diffusive fluxes occur when convection is driven by thermal and concentration gradients, and the temperature and concentration diffusivities take different values. This phenomenon has relevance for numerous applications (Turner [24]), and from a theoretical point of view presents very interesting dynamics, including chaos (Cross and Hohenberg [6], Knobloch et al. [15]). We are interested here in the case of horizontal gradients (Turner [23], Jiang et al. [13]). In this configuration, quiescent (conductive) solutions can exist when thermal and solutal buoyancy forces exactly compensate each other. This occurs only for a very particular value of the separation ratio ($S = -1$, see below), but has allowed for theoretical analysis by studying the stability of the conductive solution (Ghorayeb and Mojtabi [10], Xin et al. [26], Bardan et al. [1], Bergeon and Knobloch [4]). In recent work, we addressed this case for a small Prandtl number binary mixture, including only the Soret effect (Meca et al. [19]). Results showed a quite interesting bifurcation scenario by varying the Rayleigh number. In particular, we found an orbit that is born in a global saddle-loop bifurcation, becomes chaotic in a period doubling cascade, and disappears in a blue sky catastrophe (Shilnikov [21]). This orbit is the only stable solution in a large interval of Rayleigh numbers. In this paper we analyze this system in greater depth to determine how the scenario associated to the origin of this orbit is modified when the value of S is changed to larger (i.e. less negative) values. It is relevant to assess to what extent the dynamics depends on tuned values of the parameters, or whether it is fairly robust to these changes. Moreover, by varying a second parameter we gain access to a richer portrait of the system, obtaining bifurcation lines and points of codimension two.

Correspondence to: I. Mercader (e-mail: Isabel@fa.upc.es)

We have numerically integrated the full PDE equations in a region near $S = -1$, combining steady state solving, numerical continuation, linear stability analysis, and temporal integration. The results show that distinct bifurcations of the $S = -1$ case (namely two saddle nodes and a global saddle loop) approach each other in the region near $S = -0.9$ until only a Hopf bifurcation remains, in a scenario consistent with the unfolding of a codimension-three degenerate Takens–Bogdanov point.

The outline of this paper is as follows. In Sect. 2 we detail the model and the numerical procedure. In Sect. 3 the behavior of the system for $S = -1$ is reviewed. In Sect. 4 we extend these results by letting both Ra and S vary. Finally, the discussion of the results and some concluding remarks are presented in Sect. 5.

2 Basic equations and numerical methods

We consider the 2-D flux of a binary mixture in a rectangular cavity Ω of length d and height h. The aspect ratio $\Gamma = d/h$ has been chosen to be 2. The cavity is laterally heated, maintaining different constant temperatures at the opposed vertical boundaries. ΔT is the difference between both temperatures. On the horizontal boundaries, a linear temperature profile is imposed. All the boundaries are taken to be no-slip and with no mass flux. In these conditions the dimensionless equations in Boussinesq approximation explicitly read

$$\begin{aligned}
\partial_t \mathbf{u} + (\mathbf{u}\cdot\nabla)\mathbf{u} &= -\nabla P + \sigma\nabla^2\mathbf{u} \\
&\quad + \sigma Ra[(1+S)(-0.5 + x/\Gamma) + \theta + SC]\hat{\mathbf{z}}, \\
\partial_t \theta + (\mathbf{u}\cdot\nabla)\theta &= -v_x/\Gamma + \nabla^2\theta, \\
\partial_t C + (\mathbf{u}\cdot\nabla)C &= -v_x/\Gamma - \tau\nabla^2(\theta - C), \\
\nabla\cdot\mathbf{u} &= 0.
\end{aligned} \tag{1}$$

In these equations lengths, times and temperatures are scaled with h, $t_\kappa = h^2/\kappa$ and ΔT, respectively, κ being the thermal diffusivity. $\mathbf{u} \equiv (v_x, v_z)$ is the (dimensionless) velocity field in (x, z) coordinates, P is the pressure over the density, θ and C are deviations from a linear horizontal profile of the temperature and of the rescaled concentration of the heavier component, respectively. The dimensionless parameters are the Prandtl number $\sigma = \nu/\kappa$, the Rayleigh number $Ra = \alpha g h^3 \Delta T/\nu\kappa$ and the Lewis number $\tau = D/\kappa$, where ν denotes the kinematic viscosity, g the gravity level, α the thermal expansion coefficient, and D is the mass diffusivity. The separation ratio is defined by $S = C_0(1 - C_0)\frac{\beta}{\alpha}S_T$, where S_T is the Soret coefficient, C_0 is the actual value of the concentration of the heavier component in the homogeneous mixture, and β is the mass expansion coefficient (positive for the heavier component). Finally, boundary conditions are written as

$$\mathbf{u} = \theta = \mathbf{n}\cdot\nabla(C - \theta) = 0, \quad \text{at } \partial\Omega. \tag{2}$$

These boundary conditions are not compatible with the transformation of the Soret equations into those used by Ghorayeb and Mojtabi [10], Xin et al. [26], Bardan et al. [1], Bergeon and Knobloch [4]. Note also that Eqs. (1) together with boundary conditions (2), are invariant under a rotation π around the point $(\Gamma/2, 1/2)$ as $(x, z) \to (\Gamma - x, 1 - z)$, $(v_x, v_z, \theta, C) \to (-v_x, -v_z, -\theta, -C)$. Therefore the system is Z_2-equivariant (Kuznetsov [16]). From now on solutions invariant (non-invariant) under π will be called symmetric (non-symmetric).

Equations (1) and boundary conditions (2) have been solved by a second order time-splitting algorithm, proposed by Hugues and Randriamampianina [12], applied to a pseudo-spectral Chebyshev method. To calculate steady solutions, we have adapted a pseudoespectral first-order time-stepping formulation to carry out Newton's method, as described by Mamun and Tuckerman [17], Bergeon et al. [3], Xin and Le Quéré [25]. In the preconditioned version of Newton's iteration, the corresponding linear system is solved by an iterative technique using a GMRES package (Frayssé et al. [9]). The linear stability analysis of the steady states is conducted by computing the leading eigenvalues of the Jacobian by means of Arnoldi's method, using routines from the ARPACK package. For numerical calculations the chosen parameters have been Prandtl number $\sigma = 0.00715$ and Lewis number $\tau = 0.03$. The system has been discretized in space by using 72×48 and 90×60 mesh points in steady calculations, giving both resolutions equivalent results. For example, increasing the resolution, the Rayleigh number of the turning points varies less than a 0.1%. Temporal integration was used basically to follow orbits with very long periods, and in particular in regimes with divergent

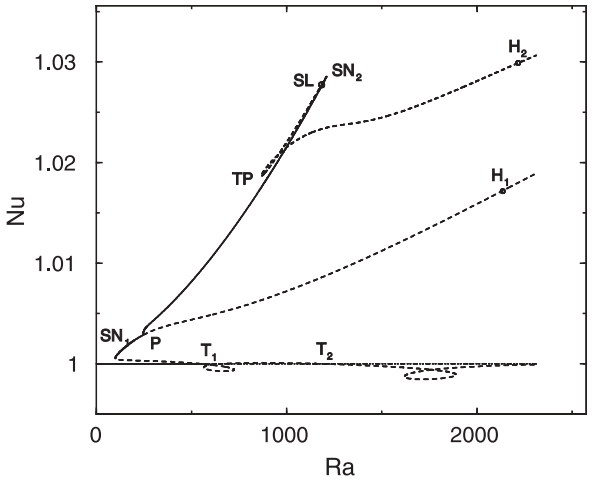

Fig. 1. Stationary solutions diagram for $S = -1$ varying Ra, as obtained by Meca et al. [19]. Continuous lines: stable states. dashed lines: unstable states

periods where a fit of the divergence itself was needed. Thus, much more computation time was required. A mesh grid of 60×30 points has proved to be sufficient to obtain results that did agree fairly well with steady calculations in the cases where the comparison applied.

3 Scenario for $S = -1$

In this section we summarize the behavior of the system for a separation ratio $S = -1$ (Meca et al. [19]). The bifurcations diagram of the steady solutions is shown in Fig. 1. In this figure, the Nusselt number Nu, defined as the ratio of the heat flux through the hot wall to that of the corresponding conductive solution, is represented as a function of the Rayleigh number Ra. For the sake of clarity, only one of the non-symmetric solutions related by π is represented. For this value of S the conductive solution is allowed. For small Ra this solution is stable, but loses stability at $Ra = 541.9$ through a transcritical bifurcation (T_1). The resulting solutions are symmetric by the rotation π, and are characterized by a central main roll accompanied by secondary ones in opposed corners. The supercritical branch is stable only until $Ra = 542.4$, where a small non-symmetric branch connects it to the conductive solutions through pitchfork bifurcations, a case analogous to that reported by Bardan et al. [1]. We center the discussion here on the solutions originating from the subcritical branch. This solution is stabilized by a saddle node bifurcation at $Ra = 99$ (SN_1) and loses stability again in a Pitchfork bifurcation at $Ra = 245$ (P), where a stable non-symmetric branch appears. In Fig. 2 (left) we see that the breaking of the symmetry confines the main roll to one lateral side. Continuing the symmetric branch, a supercritical Hopf bifurcation at $Ra = 2137$ (H_1) (maintaining symmetry) is found. At $Ra = 2253$ the bifurcating periodic solution gains stability in a Pitchfork bifurcation.

Furthermore, the steady non-symmetrical solution undergoes a saddle-node bifurcation at $Ra = 1209$ (SN_2) and has a saddle-saddle turning point at $Ra = 865.6$ (TP). Further along this branch, a Hopf bifurcation can be found at $Ra = 2218$ (H_2). A detail of this branch in the region of the two turning points is represented in Fig. 2 (right). Here, the variable E_k, related with the kinetic energy and defined as

$$E_k = \frac{1}{\Gamma} \int_{x=0}^{x=\Gamma} \int_{z=0}^{z=1} \mathbf{v}\cdot\mathbf{v}\, dxdz, \tag{3}$$

is plotted versus the Rayleigh number Ra. In this figure we have also included the sign of the real part of the leading eigenvalues; a parenthesis is used to indicate a complex conjugated pair. Between both turning points an homoclinic saddle loop connection at $Ra = 1184$ (SL) gives birth to a periodic non-symmetric solution (Meca et al. [19]). This orbit, which is the only stable solution in a wide range of values of the Rayleigh number Ra, is characterized by very long periods and a spiking behavior. In particular at the SL connection its period diverges logarithmically as expected.

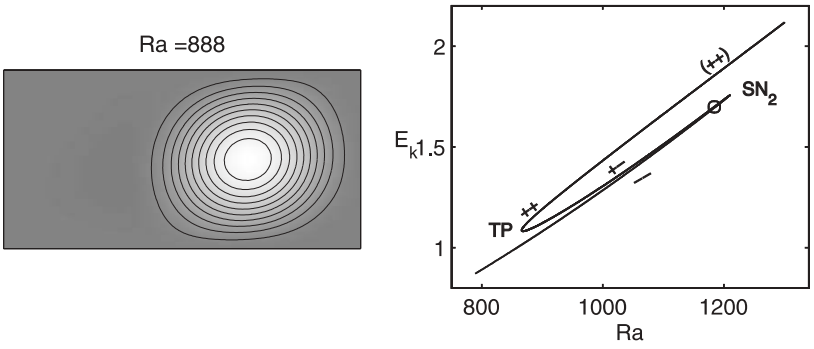

Fig. 2. Non symmetric steady solution for $S = -1$. Left: Stream lines for the stable solution at $Ra = 888$. Right: Detail of the non-symmetric branch in the region of the two turning points, indicating the sign of the real part of the leading eigenvalues. The open circle denotes a global saddle-loop bifurcation

When the Rayleigh number is increased, a very interesting complex behavior of this orbit arises (Meca et al. [19]). Firstly, at $Ra = 2137$ the orbit starts to show ripples, reflecting the frequency corresponding to the Hopf bifurcation H_1, while the period increases dramatically. In the region near $Ra = 2235$ the orbit undergoes a period doubling cascade, becoming chaotic. At $Ra = 2257.5$ the chaotic attractor disappears in a blue sky catastrophe, in a scenario similar to that proposed by Shilnikov and Turaev [22] in which both length and period of an orbit diverge at the bifurcation point.

4 Results for $S > -1$

We have performed both steady state and temporally dependent calculations of the system for different values of S above -1. We have centered our research on the solutions from which the non-symmetric orbit is born in a global saddle loop (SL) connection. Namely, we are referring to the non-symmetric branch with two successive turning points (SN_2 and TP), between which the SL connection is found. This is the situation represented in Fig. 2 (right) for $S = -1$.

This configuration of bifurcations changes when S is increased. The sequence of events in this region is quite complex, but the final situation is simple. Remarkably, for values around $S = -0.8920$ only a Hopf bifurcation remains. To analyze this process we present in Fig. 3 results for this branch and different S values. In this figure, branches and local bifurcations are found by continuing steady solutions and performing linear stability analysis, whereas global bifurcations are located by temporal integration. To do this, we fix a value of S, and starting from a periodic solution as initial condition, we vary slightly the Rayleigh number while monitoring the value of the period of the final stable orbit. Then, the connection is located at the point where the period diverges.

The first qualitative change occurs between $S = -1$ and -0.9, where the global connection SL moves toward the saddle node SN_2, becoming a SNIC (saddle node on an invariant circle) in a saddle-node separatrix-loop (SNL) codimension-two bifurcation. This change is manifested in the law of divergence of the period T found by temporal integration of the bifurcating orbit for Ra toward the homoclinic connection. The divergence for the SL is logarithmic, i.e.

$$T \sim -\frac{1}{\lambda} \log (Ra - Ra_c) + A, \tag{4}$$

where Ra_c is the value for which the global connection takes place and λ is the eigenvalue of the jacobian matrix associated to the unstable direction of the hyperbolic solution. The divergence changes to square root for the SNIC:

$$T \sim \frac{B}{\sqrt{Ra - Ra_c}} + A. \tag{5}$$

Here, Ra_c corresponds to the position of the saddle node. Furthermore, as we increase S, the point at which the two positive eigenvalues merge to become a pair of conjugated complex values (see Fig. 2 right) approaches the turning point (TP) until a Takens–Bogdanov (TB) codimension-two bifurcation occurs there for S near -0.8990. In Fig. 3 we see the branch for $S = -0.897$, for which the TB has unfolded to a Hopf

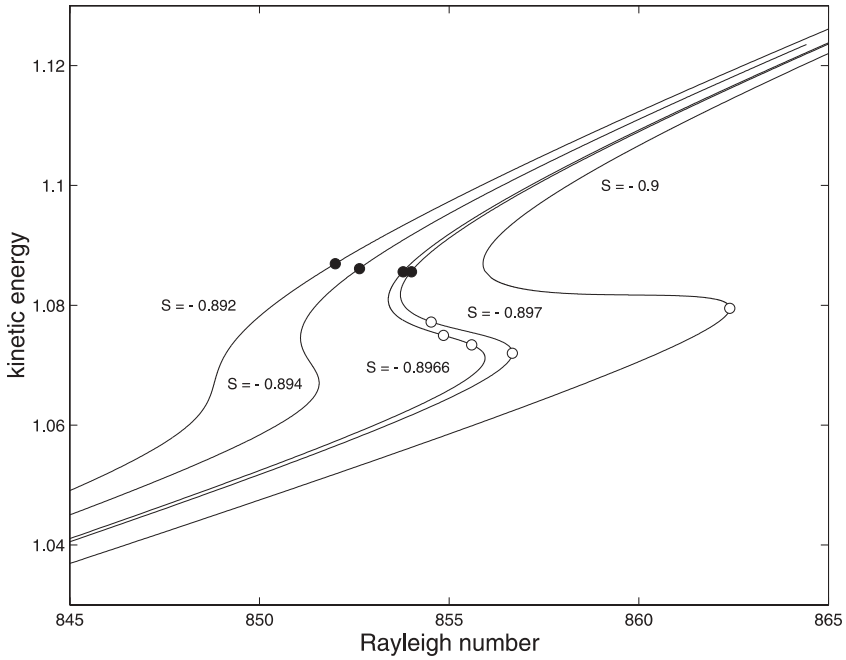

Fig. 3. Detail of the bifurcations diagram for several values of $S > -1$. Kinetic energy is represented versus Ra. Full circles denote Hopf bifurcations. Global bifurcations (either SL or SNIC) are represented by open circles

bifurcation and a global saddle loop connection, which constitute the birth and the end of an orbit that has been calculated by temporal integration. The divergence of the period of this orbit at the saddle loop is again logarithmic, as in Eq. (4). Therefore for this value of S we obtain both divergences, logarithmic for the SL and square root for the SNIC. We have performed fits of the periods for both points. Indeed, the λ value obtained by the fit, $\lambda_{fit} = 0.0173$, agrees fairly well with the eigenvalue obtained by the stability calculation of the steady state ($\lambda = 0.0166$). For the SNIC, $Ra_c(fit) = 856.64$, and the value of SN_2 is $Ra_c = 856.67$. In this situation the eigenvalue that became positive at SN_2 gains stability at TP. At the Hopf bifurcation the solution loses stability again.

When S is slightly increased, an additional codimension-two SNL bifurcation is found at SN_2, the SNIC becoming an SL moving away from the saddle node. At this moment, both SL are approaching each other, a situation represented in the branch $S = -0.8966$ in Fig. 3. The divergences of the periods of the corresponding homoclinic orbits are shown in Fig. 4. They are both logarithmic, with fitted values for the eigenvalues being $\lambda_{fit} = 0.00968$ and 0.0118, according well with the steady calculations $\lambda = 0.00820$ and 0.0134, respectively.

Very soon afterwards they touch each other and disappear. By $S = -0.894$ no global connection remains in this branch. It is now possible for the two turning points (SN_2 and TP) to annihilate each other in a codimension-two cusp bifurcation. That occurs for $S = -0.8928$. The final situation, in which only the Hopf bifurcation is found, is represented by the $S = -0.892$ branch of Fig. 3.

5 Discussion and concluding remarks

In the preceding section we have numerically studied the change of an interesting branch of non-symmetric solutions when a second parameter (the separation ratio S) is varied. The scenario that emerges from these results consists of a series of codimension-two bifurcations arranged to enable two destabilizing turning points of a branch connected to an orbit by a global bifurcation to disappear, resulting in a simpler situation with only a local Hopf bifurcation.

These results can be summarized by drawing bifurcation lines and codimension-two points in an (S, Ra) plot. This is shown in Fig. 5. In this figure the two turning point lines meet in a cusp bifurca-

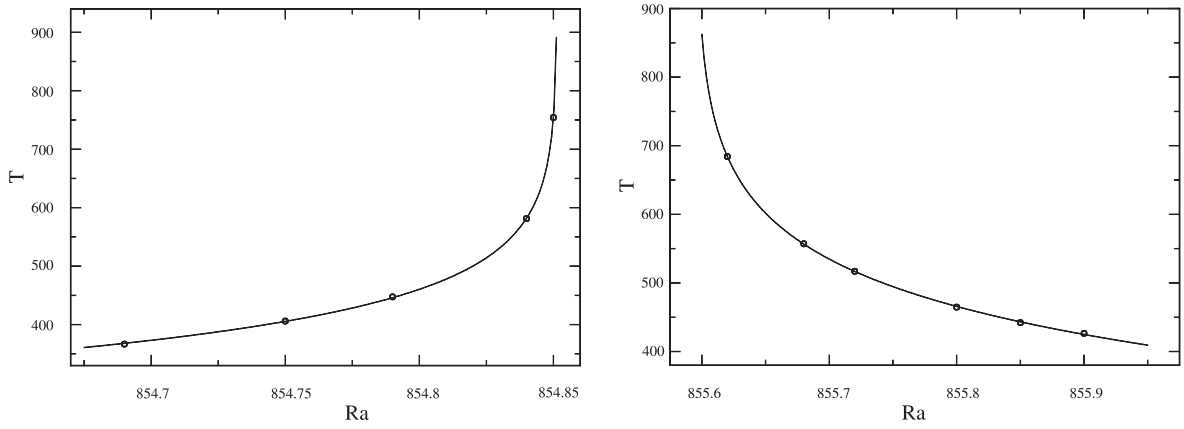

Fig. 4. Periods of the homoclinic orbits found at $S = -0.8966$ near their corresponding SL, together with the corresponding logarithmic fits. Left: divergence located at $Ra = 854.853$; Right: divergence located at $Ra = 855.595$

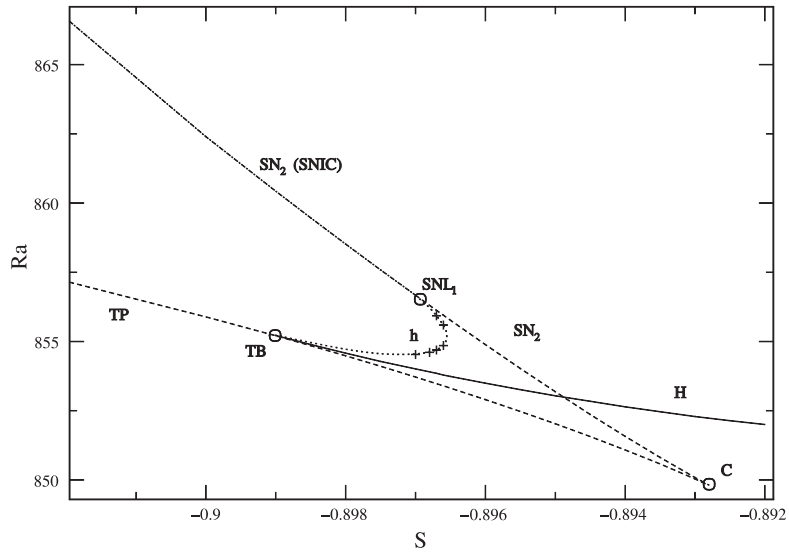

Fig. 5. Bifurcation lines in the (S, Ra) parameter space (see text)

tion at $S = -0.8928$. We can track the larger eigenvalues of the system along these lines. We find that at $S = -0.8990$ the solution on the line TP has a double zero eigenvalue. This indicates the presence of a Takens–Bogdanov (TB) codimension-two point. Indeed, this can also be checked by noting that, by performing linear stability analysis, a branch of Hopf bifurcations, with very low frequency starting from zero, also begins at this point. It should be stressed that in order for both turning points to be effectively annihilated TP should become stabilizing. That happens at the TB point.

The existence of a TB bifurcation also implies the existence of a branch of homoclinic connections (saddle-loop). This is, in fact, one of the few analytical methods of proving the existence of a homoclinic orbit. We have used the time evolution code to situate the line of homoclinic connections as detailed in Sect. 4, and checked if the period of the orbit diverges following the logarithmic law (Eq. (4)). Indeed the values found for λ_{fit} did agree well with the eigenvalues calculated from the stability of the steady solutions. The fitting of the value of Ra_c yields the points marked in Fig. 5. We see that the line that joins these points is connected with the saddle-node line corresponding to the SN_2 points. This connection is SNL_1 (located very close to $S = -0.897$), one of the saddle-node separatrix-loop points (Schecter [20]) mentioned above. It is at this point that the branch of homoclinic connections merges with the saddle-node line to become an SNIC line. This is confirmed by the change of the logarithmic law for the divergence of the period (Eq. (4)) to the square root of Eq. (5).

If we keep following the SNIC line toward more negative separation ratios, we find the other codimension-two saddle-node separatrix-loop point (SNL_2, at $S = -0.92$, not shown in Fig. 5) where the SNIC line ends, giving birth again to a homoclinic bifurcations line separated from the saddle-node line. Following this line until $S = -1$ we recover the SL point at $Ra = 1184$.

This particular configuration of codimension-two bifurcations is very far from being peculiar of this problem. It is found in many other areas, such as bursting oscillations in neural or biological systems (de Vries [7], Borisuk [5]), population dynamics (Bazykin [2]), laser dynamics (Mayol et al. [18]), and some diffusively coupled systems (Kanamami and Sekine [14]). Theoretically, all this behavior can be reproduced as a 2-dimensional slice in parameter space of the unfolding of a codimension-three degenerate Takens–Bogdanov point (Dumortier et al. [8]), also known as the Dumortier–Roussarie–Sotomayor (DRS) bifurcation. In particular, we are referring to the focus case described by Dumortier et al. [8]. This is also consistent with the fact that the presence of the SNIC cannot be related to a local codimension-2 phenomenon (Golubistky et al. [11]).

The scenario in which the DRS bifurcation appears can be described by a planar vector field (Dumortier et al [8]), i.e. it is essentially two-dimensional. This suggests the possibility of calculating the normal form coefficients of the bifurcation from the PDE's, which is an interesting problem from a theoretical point of view.

Acknowledgments. This work was financially supported by Dirección General de Investigación Científica y Técnica (Spain) (Projects BFM2003-00657 and BFM2003-07850-C03-02) and Comissionat per a Universitats i Recerca (Spain) Projects (2001/SGR/00221 and 2002/XT/00010). We also acknowledge computing support from Centre Europeu de Paral·lelisme de Barcelona (Spain). E.M. acknowledges a grant from Ministerio de Educación, Cultura y Deporte (Spain).

References

1. Bardan, G., Bergeon, A., Knobloch, E., Mojtabi, A.: Nonlinear doubly diffusive convection in vertical enclosures. Physica D **138**, 91–113 (2000)
2. Bazykin, A.: *Mathematical Biophysics of interacting populations*. Nauka, Moscow, (1985)
3. Bergeon, A., Henry, D., BenHadid, H., Tuckerman, L.S.: Marangoni convection in binary mixtures with Soret effect. J. Fluid Mech. **375**, 143–177 (1998)
4. Bergeon , A., Knobloch, E.: Natural doubly diffusive convection in three-dimensional enclosures. Phys. Fluids **14**, 3233–3250 (2002)
5. Mark Borisuk, T.: *Bifurcation Analysis of a Model of the Frog Egg Cell Cycle*. PhD thesis, Virginia Polytechnic Institute and State University, (1997)
6. Cross, M.C., Hohenberg, P.C.: Pattern formation outside of equilibrium. Rev. Mod. Phys. **65**(3), 851–1112 (1993)
7. de Vries, G.: *Analysis of the Models of Bursting Electrical Activity in Pancreatic β-Cells*. PhD thesis, University of British Columbia, (1996)
8. Dumortier, F., Roussarie, R., Sotomayor, J.: Bifurcations of Planar Vector Fields. In: *Generic 3-Parameter Families of Planar Vector Fields, Unfoldings of Saddle, Focus and Elliptic Singularities With Nilpotent Linear Parts*, Lecture Notes in Mathematics, 1480, 1–164, Springer-Verlag, (1991)
9. Frayssé, V., Giraud, L., Gratton, S., Langou, J.: A set of GMRES routines for real and complex arithmetics on high performance computers. Technical Report TR/PA/03/3, CERFACS, (2003)
10. Ghorayeb, K., Mojtabi, A.: Doubly diffusive convection in a vertical rectangular cavity. Phys. Fluids **9**, 2339–2348 (1997)
11. Golubistky, M., Josic, K., Kaper, T.J.: An unfolding theory aproach to bursting in slow-fast systems. In: H.W. Broer, B. Krauskopf, G. Vegta, editors, *Global Analysis of Dynamical Systems: Festschrift dedicated to Floris Takens on the occason of his 60th birthday*, 277–308. Institute of Physics Publications, (2001)
12. Hugues, S., Randriamampianina, A.: An improved projection scheme applied to pseudospectral methods for the incompressible Navier–Stokes equations. Int. J. Numer. Methods Fluids **28**, 501–521 (1998)
13. Jiang, H.D., Ostrach, S., Kamotani, Y.: Unsteady thermosolutal transport phenomena due to opposed buoyancy forces in shallow enclosures. J. Heat Transfer, **113**, 135–140 (1991)
14. Kanamami, T., Sekine, M.: Array enhanced coherence resonance in the difussively coupled active rotators and its analysis with the nonlinear Fokker-Plank equation. IEICE Transactions on Fundamentals, (2003)
15. Knobloch, E., Moore, D.R., Toomre, J., Weiss, N.O.: Transition to chaos in two-dimensional double-diffusive convection. J. Fluid Mech. **166**, 409–448 (1986)
16. Kuznetsov, Y.A.: *Elements of Applied Bifurcation Theory*, volume 112 of *Applied Mathematical Sciences*. Springer-Verlag, New York, 2nd edition, (1998)
17. Mamun, C.K., Tuckerman, L.S.: Asymmetry and Hopf bifurcation in spherical Couette flow. Phys. Fluids **7**, 80–91 (1995)

18. Mayol, C., Toral, R., Mirasso, C.R., Natiello, M.A.: Class a lasers with injected signal: Bifurcation set and Lyapunov potential function. Phys. Rev. A **66**, 1–12, 013 808 (2002)
19. Meca, E., Mercader, I., Batiste, O., Ramírez-Piscina, L.: Blue Sky Catastrophe in Double-Diffusive Convection. Phys. Rev. Lett. **92**, 234501 (2004)
20. Schecter, S.: The saddle-node separatrix-loop bifurcation. SIAM J. Math. Anal. **18**(4), 1142–1156 (1987)
21. Shilnikov, L.: Mathematical problems of nonlinear dynamics: a tutorial. Int. J. Bifurcation and Chaos **7**(9), 1953–2001 (1997)
22. Shilnikov, L.P., Turaev, D.V.: A new simple bifurcation of a periodic orbit of "blue sky catastrophe" type. Amer. Math. Soc. Transl. **200**(2), 165–188 (2000)
23. Turner, J.S.: A fluid dynamical model of differential and layering in magna chambers. Nature **285**, 213–215 (1980)
24. Turner, J.S.: Multicomponent convection. Ann. Rev. Fluid Mech. **17**, 11–44 (1985)
25. Xin, S., Le Quéré, P.: Linear stability analyses of natural convection in a differentially heated square cavity with conducting horizontal walls. Phys. Fluids **13**, 2529–2542 (2001)
26. Xin, S., Le Quéré, P., Tuckerman, L.: Bifurcation analysis of doubly-diffusive convection with opposing horizontal thermal and solutal gradients. Phys. Fluids **10**, 850–858 (1997)